Eur. Phys. J. B **2**, 157–167 (1998)

THE EUROPEAN PHYSICAL JOURNAL B

Cesium ordering and electron localization-delocalization phenomena in the quasi-one-dimensional diphosphate tungsten bronzes: $Cs_{1-x}P_8W_8O_{40}$

P. Foury-Leylekian[1,a], J.P. Pouget[1], M. Greenblatt[2], and E. Wang[2]

[1] Laboratoire de Physique des Solides[b], Université de Paris Sud, Bâtiment 510, 91405 Orsay Cedex, France
[2] Department of Chemistry, Rutgers, The State University of New Jersey, New Brunswick, N.J. 08903, USA

Received: 10 October 1997 / Received in final form: 11 December 1997 / Accepted: 16 December 1997

Abstract. We present a structural investigation of the $Cs_{1-x}P_8W_8O_{40}$ family of quasi-one-dimensional (quasi-1D) conductors, which exhibit intriguing charge transport properties where, for x small, the conductivity exhibits a crossover from a semiconducting to a metallic like regime when the temperature decreases. In these materials the W_4O_{18} double zig-zag chains, together with the P_2O_7 diphosphate groups, delimit channels which are partially filled with the Cs^+ ions. It is found, from an X-ray diffuse scattering investigation, that at room temperature the Cs^+ ions are locally ordered on a lattice of well-defined sites in the channel direction and not ordered between neighboring channels. These Cs^+ ions form 1D incommensurate concentration waves whose periodicity depends on the Cs^+ stoichiometry. In $CsP_8W_8O_{40}$ upon cooling, the intrachannel order increases significantly, and an interchannel order between the 1D Cs^+ concentration waves develops. But, probably because of kinetic effects, no tridimensional (3D) long range order of the Cs^+ ions is achieved at low temperature. The 3D low-temperature local order has been determined and it is found that the phase shift between the Cs^+ concentration waves minimizes their Coulomb repulsions. This local order is increasingly reduced as the Cs concentration diminishes. We interpret the intriguing features of the electrical conductivity in relationship with the thermal evolution of the Cs ordering effects. We suggest that in $Cs_{1-x}P_8W_8O_{40}$, for x small, a localization-delocalization transition of the Anderson type occurs due to the thermal variation of the Cs disorder. When x increases, the enhancement of the disorder leads to a localization of the electronic wave function in the whole temperature range measured. Finally, and probably because of the disorder, no charge density wave instability is revealed by our X-ray diffuse scattering investigation.

PACS. 61.50.Ks Crystallographic aspects of phase transformations; pressure effects – 64.70.Kb Solid-solid transitions – 71.45.Lr Charge-density-wave systems

1 Introduction

In recent years many studies have been devoted to the physical properties of transition metal oxides and bronzes [1]. Their structural anisotropy and the possibility to obtain the transition metal in a partially oxidized state have led to the discovery of several new families of low dimensional metals. Among the quasi-one-dimensional (quasi-1D) metallic Mo bronzes, superconductivity has been reported at $T_c \sim 2$ K in the Li purple bronze $Li_{0.9}Mo_6O_{17}$ and a charge-density-wave (CDW) ground state has been discovered below $T_p = 180$ K in the blue bronzes $A_{0.3}MoO_3$ (A = K, Rb, Tl). CDW ground states were also found in the quasi-two-dimensional (quasi-2D) Mo bronzes $A_{1-x}Mo_6O_{17}$ (A = Na, K, Tl; $x \sim 0$), and oxides $\gamma-$ and $\eta-Mo_4O_{11}$, and more recently in the family of monophosphate tungsten bronzes with pentagonal tunnels $(PO_2)_4(WO_3)_{2m}$ (MPTBp). All these quasi-2D materials are built with ReO_3-type slabs of corner sharing MoO_6 or WO_6 octahedra. The layers are connected along the third direction by insulating MoO_4 or PO_4 tetrahedra, which leads to a confinement of the conduction electrons in the layers.

Depending on the type of linkage achieved by the tetrahedra, different sorts of cavities are formed [2]. Pentagonal cavities are observed in $\gamma-Mo_4O_{11}$ and in the MPTBp. Hexagonal cavities are observed in $\eta-Mo_4O_{11}$ or when alkali metals are inserted in the monophosphate tungsten bronze series $A_x(PO_2)_4(WO_3)_{2m}$ (A = Na, K; $x < 1$). Such cavities are also formed in the tungsten bronze series $A_x(P_2O_4)_2(WO_3)_{2m}$ (A = K, Rb, Tl, Ba) where the insulating layers are composed of diphosphate P_2O_7 groups.

Constructed in the same manner, the MPTBp with $m = 2$ (PWO_5) exhibits however quasi-1D electronic

[a] e-mail: foury@lps.u-psud.fr
[b] CNRS-URA 02

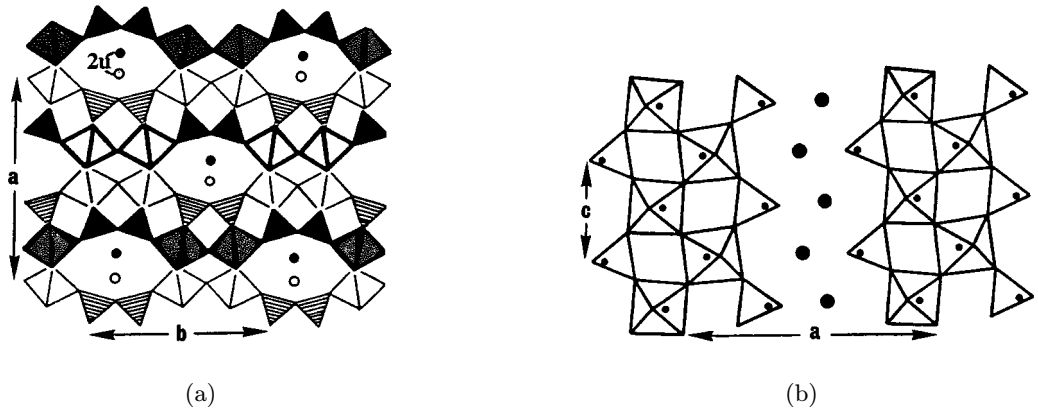

(a) (b)

Fig. 1. Structure of $Cs_{1-x}P_8W_8O_{40}$ projected along the **c** (a) and **b** (b) directions. The big circles represent the sites partially occupied by the Cs^+ ions. In (a) the filled and empty circles correspond to sites located in $z \approx 1/4$ and $z \approx 3/4$ respectively.

properties related to the fact that m is too low to link the WO_6 octahedra into layers. The structure is then composed of single zig-zag chains of octahedra. With one electron localized per W, this compound presents an antiferromagnetic ground state [2a, 3]. In the presence of Cs, the structure of PWO_5 becomes an association of double zig-zag chains separated by the P_2O_7 diphosphate groups [4]. This association creates octagonal cavities partially filled by the Cs^+ ions. The material which thus results, $Cs_{1-x}P_8W_8O_{40}$, exhibits quasi-1D metallic properties [5–7]. In addition to the quasi-1D anisotropy of the structure, and of the conduction electron system, which could lead to the formation of density-wave ground states, the interest of this last series of compounds is in the presence of large cavities, delimited by the oxide host lattice, partially filled with monovalent cations. The partial insertion of cations in such cavities allows the conduction electron density per transition metal element to be varied and the physical properties to be changed with x. Incidentally, the nonstoichiometry in the cation content can also introduce disorder in structure. In a low-dimensional metal, the disorder can strongly perturb the delocalized nature of the conduction-electron wave function [8].

In this framework we have undertaken a detailed structural study of the Cs diphosphate tungsten bronzes $Cs_{1-x}P_8W_8O_{40}$, whose average structure has been well refined [4], and whose electronic properties have been recently measured [5–7] and shown to exhibit several thermal anomalies. A preliminary report of our structural investigation can be found in reference [9].

$Cs_{1-x}P_8W_8O_{40}$, whose structure is shown Figure 1, is composed of W_4O_{18} double zig-zag chains of WO_6 octahedra running along the c direction. There are two bichains linked together by the diphosphate P_2O_7 groups per unit cell. The P-W-O host lattice has the Pcmn orthorhombic symmetry [4]. The lattice parameters depend very weakly on the Cs content and their average values amount to $a = 13.07$ Å, $b = 12.33$ Å and $c = 5.295$ Å [5]. There are two channels of octagonal cavities related by the n glide plane symmetry per unit cell. In each cavity the steric repulsions of the nearby oxygen atoms delimit well defined sites which can be occupied by the Cs. There are two such sites, separated by $c/2$, per channel period, c. With respect to the average channel direction these sites are shifted by $\pm u$ ($u = 0.038$ Å) along the a direction. They thus form zig-zag chains running along **c**. As the distance between two successive sites, $d = 2.93$ Å, is much smaller than the ionic diameter of Cs^+ (~ 4.04 Å)[1], two neighboring sites cannot be simultaneously occupied. The compound having the maximum Cs concentration is thus $Cs_2P_8W_8O_{40}$, which has not yet been synthesized. The compound with the maximum Cs concentration which has been synthesized is $CsP_8W_8O_{40}$, where only one site out of four is occupied. In this compound the Cs^+ ions are however not ordered at room temperature (RT). The characterization of the Cs^+ disorder is the first purpose of this paper.

Due to the presence of the P_2O_7 groups and of the large cavities which isolate the W_4O_{18} chains, it is expected that $Cs_{1-x}P_8W_8O_{40}$ presents quasi-1D electronic properties. In $CsP_8W_8O_{40}$ this 1D anisotropy is confirmed by electrical measurements giving a resistivity (ρ) along c, $\rho_c \approx 6 \times 10^{-3}$ Ω cm at room temperature (RT), one order of magnitude smaller than those along the a and b directions [5]. In addition, tight-binding band calculations [6,10] show that the conduction band should be dispersive only along $\mathbf{c}^*$. According to this work, which neglects the influence of the Cs^+ potential on the electron gas, $Cs_{1-x}P_8W_8O_{40}$ should be a 1D metal with a planar Fermi surface presenting a high degree of nesting by the $2k_F = \frac{1-x}{4}c^*$ wave vector [6,10] (k_F is the Fermi wave vector of the 1D electron gas).

The thermal behavior of the electrical resistivity shows that the Cs diphosphate bronzes are not conventional metals. For example the resistivity of $CsP_8W_8O_{40}$ increases

[1] This Cs^+ ionic diameter is given by R.D. Shannon, Acta Cryst. **A32**, 751 (1976), for a coordination of 12 oxygens. This value is larger in $CsP_8W_8O_{40}$ where the coordination around Cs^+ is 17 oxygens.

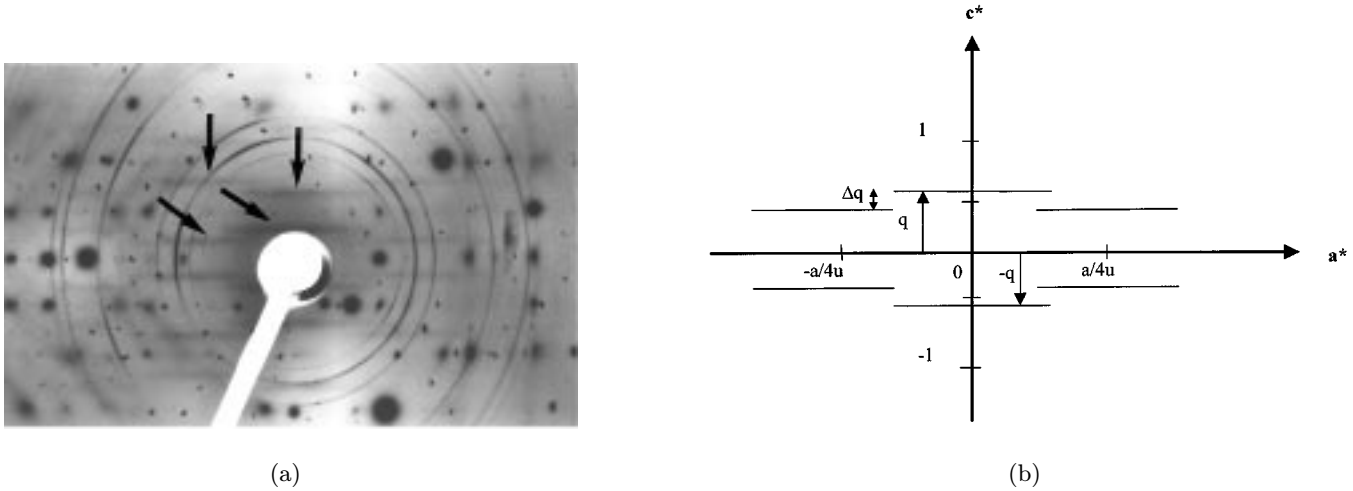

(a) (b)

Fig. 2. (a) X-ray diffraction pattern from $Cs_{0.92}P_8W_8O_{40}$ taken at room temperature using the fixed-film fixed-crystal method. The orientation is close to the (**a***, **c***) reciprocal plane. (b) Schematic representation of the X-ray pattern in the (**a***, **c***) renormalized reciprocal plane. $2u$, defined in Figure 1a, corresponds to the distance between neighboring Cs atoms, projected along **a**. In (a) the arrows point towards the diffuse lines schematically represented in (b).

upon cooling from 760 K to $T_\rho \sim 180-160$ K then decreases between T_ρ and ~ 24 K, below 24 K the resistivity steeply increases [5]. In the same temperature range the magnetic susceptibility does not reveal any significant anomaly [5]. With increasing x the temperature of the broad maximum of resistivity, T_ρ shifts to a lower value ($T_\rho \sim 100$ K for $x \sim 0.1$) and disappears for $x > 0.2$ [6]. For $x > 0.2$, the resistivity increases in the whole temperature range when the temperature decreases [6,7]. All these features show that the charge transport properties strongly depend on the Cs content. In addition the change of sign of the thermal coefficient of the electrical resistivity, at T_ρ for x small, suggests a mobility transition which could be associated with a thermal evolution of the Cs disorder. The study of this disorder as a function of temperature and Cs concentration is the second purpose of this paper.

Finally it has been suggested [6] that the steep increase of resistivity observed below 24 K could be the fingerprint of a $2k_F$ CDW ground state. The search for an eventual low-temperature Peierls distortion is the third purpose of this paper.

2 Experimental

The X-ray diffuse scattering investigation was performed with the so called fixed-crystal fixed-film method described in reference [11]. Because of the strong X-ray absorption of the single crystals investigated, MoK_α ($\lambda = 0.709$ Å) radiation was used. The incoming monochromatized beam was obtained after (002) reflection on a graphite monochromator of the X-ray beam produced either by a sealed tube or by a rotating anode. A thin Al foil was placed in front of the X-ray film in order to filter the low energy part of the fluorescence radiation coming from the Cs. The experiments were performed with crystals mounted in such a way that simple reciprocal planes, such as ($\mathbf{a}^*, \mathbf{c}^*$), were principally projected on the photographic film. For the low temperature investigation the single crystals were glued in good thermal contact with the cold finger of a closed He circuit cryocooler with temperatures regulated between room temperature (RT) and 14 K. A semi-quantitative analysis of the diffuse intensity was performed by a microdensitometer reading of the X-ray films. The single crystals studied were taken from the same batches as those investigated in references [5–7]. Several crystals with a Cs content, $1 - x$, of 1, 0.92, 0.8 and 0.54 were studied. The Cs content was determined by microprobe analysis, and found to be homogeneous within experimental errors (less than 2% weight) in a given crystal and in a given batch. The crystals used were elongated along the c direction with well defined gold-colored facets. Their typical size was ~ 2 mm along c and 0.5 mm in transverse directions.

3 Room temperature investigation of the X-ray diffuse scattering

3.1 Experimental results

Figure 2a shows an X-ray pattern taken from $Cs_{0.92}P_8W_8O_{40}$ at RT with an orientation close to the ($\mathbf{a}^*, \mathbf{c}^*$) reciprocal plane. It exhibits well defined diffuse lines, perpendicular to the $\mathbf{c}$ ($\equiv \mathbf{c}^*$) direction, which are located at $\pm q$ from the integer L layers of main Bragg reflections (see Fig. 2b). These lines correspond

Table 1. Wave vector, q, of the Cs concentration wave determined at RT in the channel direction of $Cs_{1-x}P_8W_8O_{40}$ and comparison between the Cs concentrations, $1-x$, determined by microprobe analysis and by the structural measurement of q.

	$(1-x)_{\mu\text{probe}}$	q (c^* units)	$(1-x)_{\text{struct.}} = 2q$
$CsP_8W_8O_{40}$	1 ± 0.02	0.53 ± 0.02	1.06 ± 0.04
$Cs_{0.92}P_8W_8O_{40}$	0.92 ± 0.02	0.60 ± 0.02	1.2 ± 0.04
$Cs_{0.8}P_8W_8O_{40}$	0.80 ± 0.02	0.35 ± 0.02	0.7 ± 0.04
$Cs_{0.54}P_8W_8O_{40}$	0.54 ± 0.02	0.30 ± 0.05	0.60 ± 0.1

to diffuse sheets perpendicular to $\mathbf{c}^*$ in the reciprocal space. They exhibit maxima and minima of intensity in the $\mathbf{a}^*$ direction, which give rise to the segments on the X-ray pattern shown in Figure 2a. These extrema are out of phase between two successive layers of segments, a distance of $\Delta q = 2q - 1$ along $\mathbf{c}^*$, as schematically represented Figure 2b. Similar diffuse lines were observed in $CsP_8W_8O_{40}$ and $Cs_{0.8}P_8W_8O_{40}$, with, as indicated in Table 1, a q location depending on the Cs concentration. The modulation of intensity of the diffuse lines along $\mathbf{a}^*$ was however found to be independent of the Cs content. A very broad and nearly undetectable diffuse scattering was also observed in $Cs_{0.54}P_8W_8O_{40}$ at RT.

This diffuse scattering traduces a correlated disorder in the structure which depends on the Cs content and which thus can be related to the occupancy of the Cs^+ ions in the octagonal channels. The observation of diffuse lines perpendicular to the $\mathbf{c}$ direction suggests a Cs disorder uncorrelated from channel to channel, together with a partial order along the channel direction. In the next section we shall encounter the observed diffuse scattering intensity by the calculation of the diffraction from an assembly of independent channels made of zig-zag sites partially filled by Cs^+ ions.

3.2 Intensity diffracted by a Cs channel

With respect to an origin situated in the middle of one arm of the zig-zag, the position of the nth site ($n = 1, 2$) accessible by the Cs^+ ions in the lth unit cell of a channel is:

$$\mathbf{r}_{ln} = l\mathbf{c} + (-1)^n(\mathbf{u} + \mathbf{c}/4) \tag{1}$$

where $\mathbf{u}$ is half the amplitude of the zig-zag shown in Figure 1b ($\mathbf{u} // \mathbf{a}$). The amplitude diffracted by a channel is given by:

$$A_{1\text{D}}(\mathbf{Q}) = \sum_{l,n} f_{ln}(\mathbf{Q}) \exp(i\mathbf{Q}\,\mathbf{r}_{ln}) \tag{2}$$

where $\mathbf{Q}$ is the scattering wave vector and:

$$f_{ln}(\mathbf{Q}) = \mathrm{f}_{\mathrm{Cs}}(\mathbf{Q})$$

if the site is occupied by a Cs^+ ion of form factor $f_{\mathrm{Cs}}(\mathbf{Q})$,

$$f_{ln}(\mathbf{Q}) = 0$$

if the site is empty.

If one groups together the 2 sites of the lth unit cell, the expression (2) becomes:

$$A_{1\text{D}}(\mathbf{Q}) = \sum_{l} F_l(\mathbf{Q}) \exp(il\mathbf{Q}\mathbf{c}) \tag{3}$$

where

$$F_l(\mathbf{Q}) = f_{l1}(\mathbf{Q}) \exp[-i\mathbf{Q}(\mathbf{u} + \mathbf{c}/4)] + f_{l2}(\mathbf{Q}) \exp[i\mathbf{Q}(\mathbf{u} + \mathbf{c}/4)] \tag{4}$$

is the structure factor of the lth unit cell. The intensity diffracted by a channel is thus:

$$I_{1\text{D}}(\mathbf{Q}) = \sum_{l,m} F_{l+m}(\mathbf{Q}) F_l(\mathbf{Q})^* \exp(im\mathbf{Q}\mathbf{c})$$

and the intensity diffracted outside the Bragg reflections is given by [12]:

$$\delta I_{1\text{D}}(\mathbf{Q}) = N \sum_{m} [\langle F_{l+m}(\mathbf{Q}) F_l(\mathbf{Q})^* \rangle - |\langle F \rangle|^2] \exp(im\mathbf{Q}\mathbf{c}) \tag{5}$$

where $\langle\ \rangle$ means a spatial average and N is the number of unit cells. In the expression (5), $\langle F \rangle$ is the spatial average of expression (4):

$$\langle F \rangle = 2C f_{\mathrm{Cs}}(\mathbf{Q}) \cos[\mathbf{Q}(\mathbf{u} + \mathbf{c}/4)] \tag{6}$$

where C is the average occupancy of one Cs site; $C = (1-x)/4$ (the factor 4 comes from the fact that there are two sites available per channel and two channels per one chemical formulae unit cell). The structure factor (4) can be put in the form:

$$F_l(\mathbf{Q}) = f_{\mathrm{Cs}}(\mathbf{Q})\{[\sigma(l1)] \exp[-i\mathbf{Q}(\mathbf{u} + \mathbf{c}/4)] + [\sigma(l2)] \exp[i\mathbf{Q}(\mathbf{u} + \mathbf{c}/4)]\} \tag{7}$$

where $\sigma(ln)$ is a function describing the modulation of occupancy of the site $\mathbf{r}_{ln}$, with respect to its average occupancy C. The experimental observation of $\pm q$ diffuse lines shows that there is partial order of the Cs^+ ions along the c direction with the periodicity $\lambda = 2\pi/q$ ($\lambda = c/2C = 2c/(1-x)$ corresponds to the average distance between two Cs^+ ions in the channel direction). Assuming that $\sigma(ln)$ varies spatially with this wave length, one can pose that for the two sites of the lth unit cell, with respect to its origin:

$$\sigma(l1) = C + \Sigma(l, q) \exp(\mp i\mathbf{q}\mathbf{c}/4) \tag{8a}$$

and

$$\sigma(l2) = C + \Sigma(l, q) \exp(\pm i\mathbf{q}\mathbf{c}/4). \tag{8b}$$

In the expressions (8) it is assumed that $\Sigma(l,q)$, the amplitude of modulation of the lth unit cell, remains the same on the two sites, which means that the modulation wave does not decay on $c/2$ (*i.e.* that $\xi_{//} > c/2$ — see below). These quantities included in the expression (7) lead to:

$$F_l(\mathbf{Q}) = \langle F\rangle + 2f_{\mathrm{Cs}}(\mathbf{Q})\Sigma(l,q)\cos[\mathbf{Qu} + (\mathbf{Q}\pm\mathbf{q})\mathbf{c}/4]. \tag{9}$$

The diffuse intensity thus becomes:

$$\delta I_{1\mathrm{D}}(\mathbf{Q}) = 4N|f_{\mathrm{Cs}}(\mathbf{Q})|^2\cos^2[\mathbf{Qu} + (\mathbf{Q}\pm\mathbf{q})\mathbf{c}/4] \times \sum_m \langle\Sigma(l+m,q)\Sigma(l,q)^*\rangle\exp(im\mathbf{Qc}). \tag{10}$$

In expression (10) $\langle\Sigma(l+m,q)\Sigma(l,q)^*\rangle$ represents the q component of the Cs-Cs occupancy correlation function between two unit cells separated by $m\mathbf{c}$. This quantity can also be written in the form:

$$\langle\Sigma(l+m,q)\Sigma(l,q)^*\rangle = CP_{\mathrm{Cs-Cs}}(m,q) \tag{11}$$

where $P_{\mathrm{Cs-Cs}}(m,q)$ is the q component of the probability $P_{\mathrm{Cs-Cs}}(m)$ that two unit cells, $m\mathbf{c}$ apart, are simultaneously occupied by a Cs^+ ion. In order to calculate this probability we have assumed that only the $\pm q$ components of amplitude P_q are necessary to describe the Cs concentration wave. This approximation is reasonable because the diffuse lines located at the positions $\pm nq$ of the other Fourier components are not observed. In addition we assume that the Cs order remains limited in the c direction and that its spatial decay is described by a 1D Ornstein-Zernicke law involving the correlation length $\xi_{//}$. $P_{\mathrm{Cs-Cs}}(m,q)$ can thus be put in the form:

$$P_{\mathrm{Cs-Cs}}(m,q) = P_q\exp(\pm imqc)\exp(-|m|c/\xi_{//}). \tag{12}$$

With (11) and (12), expression (10) becomes:

$$\delta I_{1\mathrm{D}}(\mathbf{Q}) = 4NP_q|f_{\mathrm{Cs}}(\mathbf{Q})|^2\cos^2[\mathbf{Qu} + (\mathbf{Q}\pm\mathbf{q})\mathbf{c}/4] \times \sum_m \exp(im\mathbf{Qc})\exp(\pm imqc)\exp(-|m|c/\xi_{//}). \tag{13}$$

The summation on m leads to:

$$\delta I_{1\mathrm{D}}(\mathbf{Q}) \propto |f_{\mathrm{Cs}}(\mathbf{Q})|^2\cos^2[\mathbf{Qu} + (\mathbf{Q}\pm\mathbf{q})\mathbf{c}/4] \times \sum_L \frac{1}{[(Q_c\pm q) - Lc^*]^2 + \xi_{//}^{-2}}\cdot \tag{14}$$

In (14), Q_c is the component of $\mathbf{Q}$ along the channel direction, L are the Miller indices along c^*. The diffuse scattering $\delta I_{1\mathrm{D}}(\mathbf{Q})$ consists of diffuse sheets located at $Q_c = Lc^* \mp q$. Its intensity is modulated by the square of the structure factor of the lattice of sites:

$$\cos^2[\mathbf{Qu} + (\mathbf{Q}\pm\mathbf{q})\mathbf{c}/4] = \cos^2[\mathbf{Qu} + L\pi/2]. \tag{15}$$

This function has a period π/u along a^* and is respectively out of phase for the $\pm q$ sheets associated to the L even and L odd layers of main Bragg reflections perpendicular to the c direction. This is exactly what is observed (see Fig. 2). Furthermore from the $2\pi/2u$ periodicity along a^* of the diffracted experimentally observed intensity one deduces $u \sim 0.04$ Å. This value is in excellent agreement with the one, $u = 0.038$ Å, deduced from the structural refinements [4]. The overall intensity of the diffuse scattering behaves as the square of the Cs form factor, $|f_{\mathrm{Cs}}(\mathbf{Q})|^2$, which decreases when $|\mathbf{Q}|$ increases. This explains why the diffuse sheets are well observed only near the origin of the reciprocal space, where $\mathbf{Q}$ is small.

The measure of the reduced wave vector of the diffuse sheets, $q = \frac{1-x}{2}c^*$, allows the determination of the Cs stoichiometry, $1-x$. Table 1 shows that there is good agreement between the microprobe and structural determinations of $1-x$ for the $CsP_8W_8O_{40}$, $Cs_{0.8}P_8W_8O_{40}$ and $Cs_{0.54}P_8W_8O_{40}$ samples. This is not the case for the $Cs_{0.92}P_8W_8O_{40}$ sample investigated where the structural stoichiometry is found to be close to 1.2. The difference between the microprobe and structural stoichiometry of this sample is not understood.

In this section we have assumed that there is, at RT, a short range order of the Cs^+ ions in the channel direction. The observation of diffuse sheets broader than the experimental resolution along $\mathbf{c}^*$ confirms this assumption. In the next section we shall analyze more quantitatively this broadening. Expression (14) predicts that the diffuse lines have a Lorentzian profile, whose half width at half maximum (HWHM) amounts to $\xi_{//}^{-1}$.

In conclusion, the Cs sublattice, where the ions at RT occupy well defined site positions delimited by the host lattice structure $P_8W_8O_{40}$, can be viewed as a 1D liquid of sites where the disorder is due to the fractional occupation of these site positions. This 1D disorder (of the first type, according to Ref. [12]) leads, as shown by the expression (14), to the formation of diffuse sheets whose HWHM does not depend on the sheet indices. This is different from what is observed in materials such as $Hg_{3-\delta}AsF_6$ [13] or $TTT_2I_{3-\delta}$ and $DIPS\phi_4(I_3)_{0.76}$ [14][2], where the site positions are not so well defined in the channel direction. In these last compounds, the Hg^+ or the I_3^- ions form 1D liquids at RT, whose first neighbor average periodicity is incommensurate with the periodicity of the host lattice, and where the disorder is due to positional fluctuations between neighboring ions. This 1D disorder (of the second type, according to Ref. [12]) leads to the formation of diffuse sheets whose HWHM increases with the sheet indices.

4 Low-temperature investigation of the X-ray diffuse scattering

4.1 Thermal evolution of the ordering

Upon cooling, the diffuse lines, described in the last section, condense into diffuse spots as shown Figure 3. At

[2] TTT is tetrathiotetracene; $DIPS\phi_4$ is tetraphenyldithiapyranylidene.

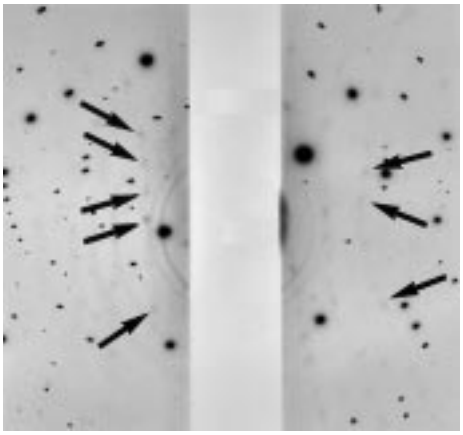

Fig. 3. X-ray diffraction pattern from $Cs_{0.92}P_8W_8O_{40}$ at 14 K. The **c*** direction is horizontal. The arrows point towards the weak and broad satellite reflections emerging from the diffuse lines.

low temperature, the width of the diffuse spots strongly depends on the Cs concentration of the sample, $1-x$. For low values of $1-x$, in particular for $Cs_{0.54}P_8W_8O_{40}$, the diffuse spots remain very broad and of weak intensity even at 14 K. For $CsP_8W_8O_{40}$, the diffuse spots are sharp, but broader than the experimental resolution, and significantly more intense than those of $Cs_{0.54}P_8W_8O_{40}$.

It is possible, except perhaps for $Cs_{0.54}P_8W_8O_{40}$, to define a temperature T_s, around 180 K, at which the spots begin to emerge from the diffuse lines. The apparition of these spots means a local ordering of the Cs^+ ions between the channels of octagonal cavities. The measurement of the HWHM of these diffuse spots in intrachannel and interchannel directions makes it possible to quantify the spatial extent of the Cs order, as we shall see below.

Figure 4 shows the thermal dependence of the peak intensity of the diffuse spots $I(T)$ for different Cs concentrations. Figures 5 and 6 represent for the same samples the thermal dependence of the HWHM of the spots along the channel direction, $\delta q_{//}(T)$, and in the perpendicular direction, $\delta q_{\perp}(T)$. The thermal behavior of each quantity depends significantly on the Cs concentration.

The profile of the spots, both in longitudinal (channel) and transverse directions, can be fitted by a Lorentzian curve, which confirms that the Cs position-position correlation function is well described by the Ornstein-Zernicke law. In all the temperature ranges, it has been checked that the integrated intensity of the diffuse spots $I(T) \times \delta q_{//}(T) \times \delta q_{\perp}(T)$ remains constant, as expected from the conservation of the number of Cs^+ ions in each sample.

The data obtained with $CsP_8W_8O_{40}$, and shown in Figures 4, 5 and 6, allow us to clearly define three temperature ranges:

- The first one takes place at temperatures higher than T_s. $I(T)$ and $\delta q_{//}(T)$ are then nearly constant in temperature, while $\delta q_{\perp}(T)$ cannot be measured. This means that, as at RT, the Cs^+ ion occupation probabilities are uncorrelated from channel to channel.
- Below T_s, $\delta q_{\perp}(T)$ can be measured. T_s can thus be defined as the temperature at which the intrachain Cs ordering begins to develop. When T decreases between T_s and about 100 K, $I(T)$ increases rapidly while $\delta q_{//}(T)$ and $\delta q_{\perp}(T)$ decrease rapidly.
- In the third temperature range, below about 100 K, the values of $I(T)$, $\delta q_{//}(T)$ and $\delta q_{\perp}(T)$ saturate. Even at 14 K, the lowest temperature investigated $\delta q_{//}(T)$ and $\delta q_{\perp}(T)$ are larger than the experimental resolution. Only a local Cs^+ ordering is achieved at this temperature.

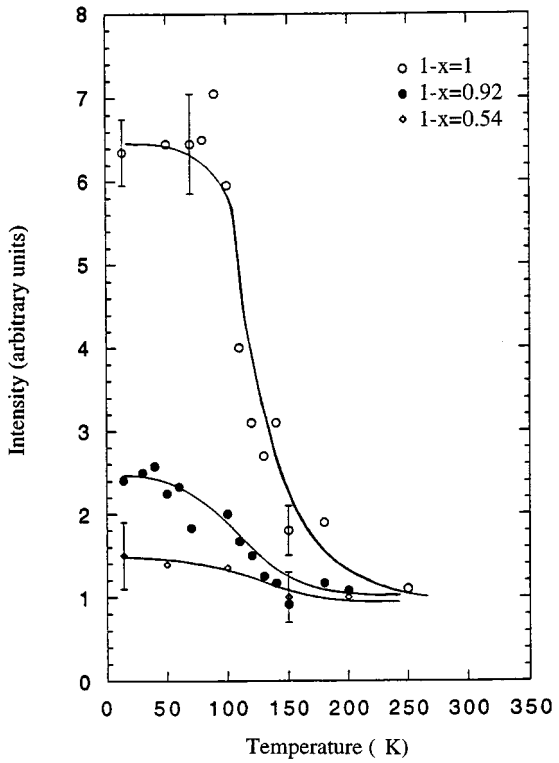

Fig. 4. Thermal variations of the peak intensity of the broad satellite reflections observed in $CsP_8W_8O_{40}$, $Cs_{0.92}P_8W_8O_{40}$ and $Cs_{0.54}P_8W_8O_{40}$. These intensities have been normalized at their 250 K value.

The thermal variations of $I(T)$, $\delta q_{//}(T)$ and $\delta q_{\perp}(T)$ strongly diminish when, as shown respectively by Figures 4, 5 and 6, the Cs concentration decreases. Very weak thermal variations are observed in $Cs_{0.54}P_8W_8O_{40}$. The low temperature values of $I(T)$, $\delta q_{\perp}(T)$ and $\delta q_{//}(T)$ strongly vary with the Cs concentration. Above T_s, $\delta q_{//}$ is the same within experimental errors in $CsP_8W_8O_{40}$ and in $Cs_{0.92}P_8W_8O_{40}$, and only slightly smaller than in $Cs_{0.54}P_8W_8O_{40}$.

The correlation lengths $\xi_{//}$ and $\xi_{\perp}$ can be deduced from the inverse of the intrinsic HWHM obtained after correction of the experimental HWHM by the Gaussian resolution. The correlation lengths thus obtained are given, at selected temperatures, in Table 2. Figure 7 gives

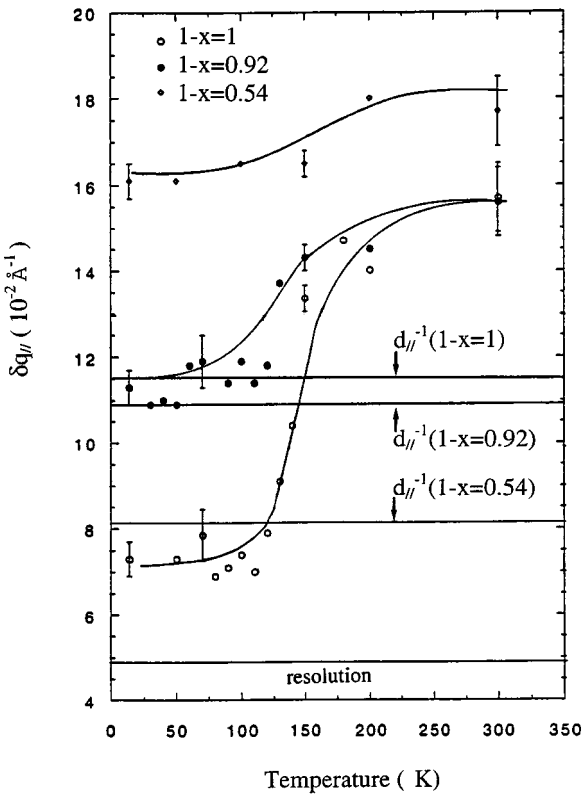

Fig. 5. Thermal variations of the half width at half maximum (HWHM) of the diffuse spots along the $\mathbf{c}^*$ direction ($\Delta q_{//}(T)$) in $CsP_8W_8O_{40}$, $Cs_{0.92}P_8W_8O_{40}$ and $Cs_{0.54}P_8W_8O_{40}$. The inverse of the average Cs-Cs distance (calculated from the microprobe concentration), $d_{//}^{-1}$, augmented by the resolution effects, is also indicated.

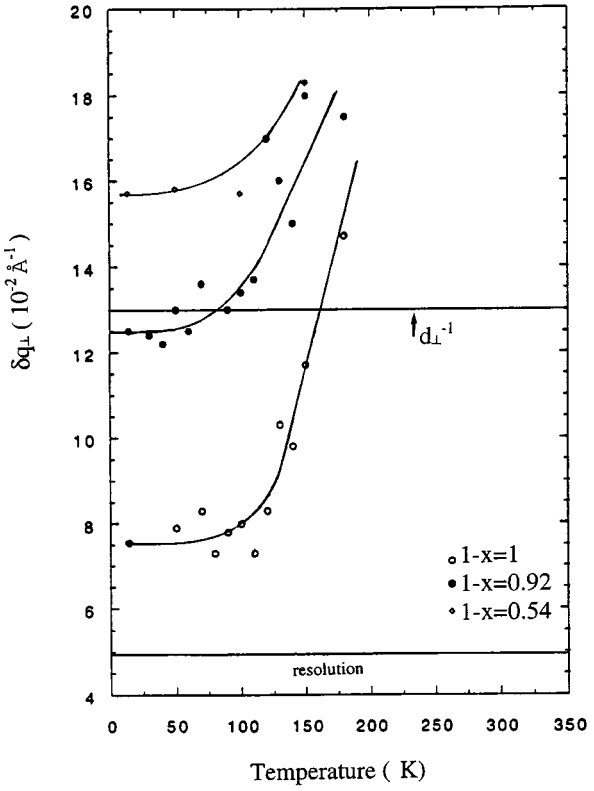

Fig. 6. Thermal variations of the half width at half maximum (HWHM) of the diffuse spots along the perpendicular to the $\mathbf{c}^*$ direction ($\Delta q_{\perp}(T)$) in $CsP_8W_8O_{40}$, $Cs_{0.92}P_8W_8O_{40}$ and $Cs_{0.54}P_8W_8O_{40}$. The inverse of the first neighbor interchannel distance, $d_{\perp}^{-1}$, augmented by the resolution effects, is also indicated.

Table 2. Cs-Cs correlation length in the intrachannel ($\xi_{//}$) and interchannel ($\xi_{\perp}$) directions of $Cs_{1-x}P_8W_8O_{40}$ at selected temperatures.

	$\xi_{//}$ (Å)		$\xi_{\perp}$ (Å)	
T(K)	300 K	14 K	180 K (*150 K)	14 K
$CsP_8W_8O_{40}$	7.2 ± 0.5	25 ± 3.5	7.7 ± 0.5	23.5 ± 3.5
$Cs_{0.92}P_8W_8O_{40}$	7.1 ± 0.5	11 ± 0.60	6.2 ± 0.4	9.5 ± 0.6
$Cs_{0.54}P_8W_8O_{40}$	6.2 ± 0.4	6.9 ± 0.2	$^*5.9 \pm 0.4$	7.10 ± 0.5

Table 3. Average distance ($d_{//}$) between the Cs atoms along the channel direction of $Cs_{1-x}P_8W_8O_{40}$. For $Cs_{0.92}P_8W_8O_{40}$ the two values of $d_{//}$ are respectively calculated for the microprobe ($d_{//} = 2c/1-x$) and structural ($d_{//} = 2\pi/q$) stoichiometries given in Table 1.

	$d_{//}$ (Å)
$CsP_8W_8O_{40}$	$\sim 2c \sim 10.6$
$Cs_{0.92}P_8W_8O_{40}$	$\sim 2c/0.9 \sim 11.5$
	$\sim 2c/1.1 \sim 9.5$
$Cs_{0.54}P_8W_8O_{40}$	$\sim 2c/0.54 \sim 19.6$

the thermal dependence of $\xi_{//}^{-1}$ and $\xi_{\perp}^{-1}$ in $CsP_8W_8O_{40}$. Table 3 gives the average Cs-Cs distance along the channel direction, $d_{//} \equiv \lambda$ ($2\pi/\lambda$ is the periodicity of the diffuse lines). This quantity will be compared with $\xi_{//}$ below. The first neighbor interchannel distance to compare with $\xi_{\perp}$ is $d_{\perp} = 8.96$ Å, the $(\mathbf{a}+\mathbf{b})/2$ distance.

For $CsP_8W_8O_{40}$[3] $\xi_{//}$ is smaller than $d_{//}$ between T_s and RT. This means that there are weak, but finite, correlations between the Cs positions, decreasing as $\exp(-r/\xi_{//})$ in the 1D Ornstein-Zernicke model. $\xi_{\perp}$ is not measurable, which means that there is no order between the Cs occupation waves located in different channels. Between T_s and 110 K , $\xi_{//}$ and $\xi_{\perp}$ increase with decreasing temperature, becoming larger than $d_{//}$ and $d_{\perp}$ below 140 K and 160 K respectively. Figure 7 shows that below about 170 K $\xi_{//}$ and $\xi_{\perp}$ are equal within experimental errors, and that below 110 K these quantities saturate, leading to a (frozen) isotropic short-range Cs order, with $\xi_{//} \approx 2d_{//}$ and $\xi_{\perp} \approx 2.5d_{\perp}$.

[3] The low temperature and the RT measurements have been performed on two different samples from the same batch.

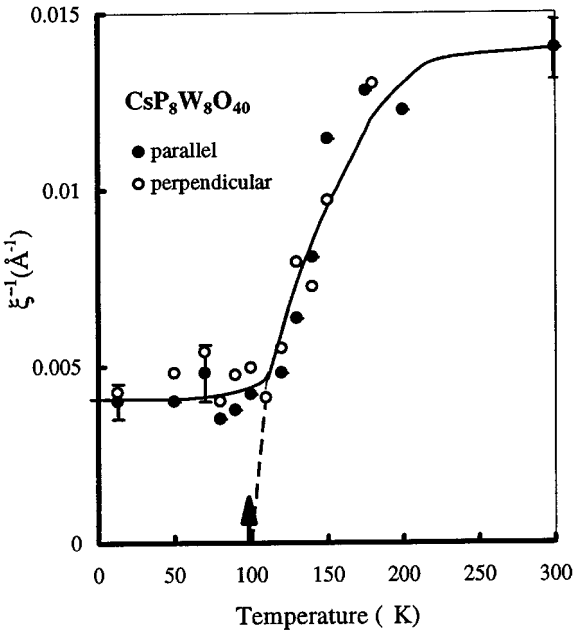

Fig. 7. Thermal variations of $\xi_{//}^{-1}$ and $\xi_{\perp}^{-1}$ in $CsP_8W_8O_{40}$. The square root extrapolation (dashed line) allows to define, according to equation (18), a virtual transition temperature T_c of 100 K.

For $Cs_{0.92}P_8W_8O_{40}$, the data show a similar behavior as that for $CsP_8W_8O_{40}$. At high temperature $\xi_{//}$ tends to the same value in both compounds. However when T decreases, the temperature evolution of $\xi_{//}$ and $\xi_{\perp}$ is smoother than for $CsP_8W_8O_{40}$. At low temperature a frozen 3D isotropic short range Cs order occurs, with $\xi_{//}$ comparable to $d_{//}$ and $\xi_{\perp}$ slightly greater than $d_{\perp}$.

In $Cs_{0.54}P_8W_8O_{40}$ nearly no thermal evolution of $\xi_{//}$ and $\xi_{\perp}$ is observed. Within experimental errors these two correlation lengths are identical. $\xi_{//}$ is more than twice smaller than $d_{//}$, while $\xi_{\perp}$ is slightly less than $d_{\perp}$.

4.2 Low temperature structure

At low temperature, the position of the broad satellite reflections in reciprocal space can be indexed by the wave vector $\mathbf{q}_s = [ha^*, kb^*, (l \pm q)c^*]$, where h, k and l are integers. These reflections are observed with the extinction condition: $h+k = 2n$. The integer components of the wave vector $\mathbf{q}_s$ in the $(\mathbf{a}^*, \mathbf{b}^*)$ reciprocal plane mean that the Cs sublattice adopts the periodicity of the channel in the $(\mathbf{a}, \mathbf{b})$ plane. This leads to the schematic representation of Figure 8, where there is no phase difference between Cs occupation waves from channels separated by the translation vectors $\mathbf{a}$ and $\mathbf{b}$. On the other hand the phase difference, ϕ for the Cs occupation waves belonging to channels separated by $(\mathbf{a}+\mathbf{b})/2$, must be π in order to account for the extinction condition previously quoted. Indeed in the centered unit cell of channels, the structure factor of the 3D lattice of Cs ordered waves can be simply written in

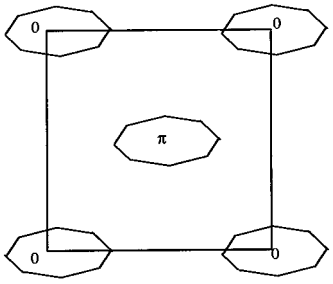

Fig. 8. Schematic representation of the low temperature $Cs_{1-x}P_8W_8O_{40}$ unit cell projected along the **c** axis. The octagonal cavities are represented together with the phase of the individual Cs concentration waves located inside these cavities.

the form :

$$F_{3D}(\mathbf{Q}) = F_{1D}(\mathbf{Q})\{1 + \exp i[(h+k)\pi + \phi]\} \qquad (16)$$

where :

$$F_{1D}(\mathbf{Q}) = 2f_{Cs}(\mathbf{Q})\sqrt{CP_q}\cos[\mathbf{Qu} + (\mathbf{Q} \pm \mathbf{q})\mathbf{c}/4] \qquad (17)$$

is the structure factor of the Cs zig-zag chain, previously calculated in Section 3.2. It is thus easy to see that $F_{3D}(\mathbf{Q}) = 0$ for $h + k = 2n$ if $\phi = \pi$.

The transverse ordering can be simply understood if one assumes that the interchannel order is due to Coulomb interactions between the Cs^+ ions, and if one considers the atomic environment of each octagonal channel in the **a**, **b** and $(\mathbf{a}+\mathbf{b})/2$ directions. The first neighbor channels along the $(\mathbf{a}+\mathbf{b})/2$ direction are separated by "insulating" PO_4 tetrahedra while the second neighbor channels along the **a** and **b** directions are separated by "metallic" WO_6 bichains. Direct Coulomb interactions along $(\mathbf{a}+\mathbf{b})/2$ tend to impose a phase difference of π between the Cs concentration waves, while Coulomb interactions along **a** and **b**, mediated by the polarizable WO_6 bichains, will impose a phase difference of 0. The order thus shown in Figure 8 is that, which minimizes the interchannel Coulomb interactions in all these directions.

4.3 Search for additional diffuse scattering below 24 K

X-ray patterns were taken down to 14 K in order to detect the presence of new diffuse scattering features which could be associated to a further structural modification around 24 K, such as the onset of the CDW transition suggested in reference [6] from the observation of a low-temperature increase of the electrical resistivity. However all our attempts to detect additional diffuse lines or diffuse spots were unsuccessful for all the concentrations studied. This allows us to exclude in particular a $2k_F$-CDW instability which would give rise to a diffuse scattering at the $q/2$ reduced wave vector.

5 Discussion

5.1 Concentration and thermal dependences of the cesium disorder

In all the samples investigated it is found that at high temperature (*i.e.* above T_s) the Cs^+ ions are only weakly ordered in the channel direction. At RT, $\xi_{//} \approx 1.5c$ does not vary significantly with the Cs concentration. $\xi_{//}$ is smaller than the average Cs-Cs distance, $d_{//}$. In $CsP_8W_8O_{40}$ $\xi_{//}$ amounts to 2/3 of $d_{//}$ at RT. As $d_{//}$ increases as $(1-x)^{-1}$, the ratio $\xi_{//}/d_{//}$ decreases with the Cs content.

In $CsP_8W_8O_{40}$ and $Cs_{0.92}P_8W_8O_{40}$ there is a net increase of $\xi_{//}(T)$ below T_s. The improvement of the intrachain Cs order has to be associated with the onset of the interchannel coupling. Upon cooling below T_s, $\xi_\perp$ rapidly increases and becomes nearly identical to $\xi_{//}$ below T^* (T^* is defined by (21) and depends on the Cs concentration). Then $\xi_{//}$ and $\xi_\perp$ exhibit about the same thermal increase. The anisotropy of the Cs local order has thus changed on crossing T_s. The improvement of the interchannel coupling below T_s could be associated with the evolution of the charge transport properties observed in the same temperature range (see Sect. 5.2).

The improvement of the intrachain Cs order requires a diffusion of the Cs^+ ions on the zig-zag lattice of sites. The Cs local order is probably achieved by the Coulomb repulsions between the Cs^+ ions both in channel direction and between neighboring channels. As we have already seen, the interchannel repulsions seem to be relevant below T_s, for x small. The Coulomb repulsions will diminish when, for x increasing, the average separation between the Cs^+ ions will increase. In addition when x increases, it will be more and more difficult for an incommensurate concentration of Cs^+ ions to achieve a sizeable intrachain order by placing the Cs^+ on a commensurate lattice of sites, because this requires the establishment of a periodic distribution of occupancy defects. Both features could qualitatively explain why the extent of the Cs^+ order decreases when $1-x$ decreases. Also the diffusion of a Cs^+ ion from one site to one of the two first neighboring sites requires the crossing of the bottleneck created in the P-W-O structure by the PO_4 tetrahedra. Such a crossing requires the opening of the bottleneck by the lattice vibrations of the host lattice. This process will be achieved at high temperature, say above 100 K, when there are enough phonons excited. At low temperature the rigidification of the host lattice structure will stop this diffusion process, leading to the freezing of the Cs local order. Such a freezing is clearly observed in $CsP_8W_8O_{40}$ below 110 K.

Above the freezing temperature of 80-110 K (depending slightly on the Cs concentration), the X-ray data can be analyzed in the framework of the theory of the 2nd order phase transition where the thermal increase of $\xi_{//} \sim \xi_\perp$ (noted ξ below) and of $I(T)$ is due to the onset of critical collective fluctuations in order to achieve a long-range order of the Cs^+ ions. However, because of the freezing of the diffusion process of individual Cs^+, the critical temperature T_c of the order-disorder transition, which would result from the Cs^+-Cs^+ interactions, cannot be reached. Figure 7 shows the thermal dependence of the inverse correlation length ξ^{-1} of $CsP_8W_8O_{40}$. Above the freezing temperature $\xi^{-1}(T)$ exhibits a thermal evolution in agreement with the mean field power law behavior:

$$\xi^{-1} \propto (T - T_c)^{1/2}. \tag{18}$$

The extrapolation of this dependence below 110 K, leads to a virtual transition at a T_c of about 100 K. In the classical limit the $\mathbf{q}_s$ peak intensity $I(T)$ behaves as:

$$I(T) \propto k_B T \chi(T) \tag{19}$$

where $\chi(T)$ is the susceptibility associated with the order parameter. In the mean field approximation, $\chi(T)$ exhibits a Curie-Weiss behavior:

$$\chi(T) \propto (T - T_c)^{-1}. \tag{20}$$

Figure 9 shows, in $CsP_8W_8O_{40}$ and in $Cs_{0.92}P_8W_8O_{40}$, that the inverse of this quantity, $T/I(T)$, roughly behaves as $T - T_c$. This allows the determination, by linear extrapolation, a T_c of respectively ~ 90 K and ~ 70 K. In $CsP_8W_8O_{40}$ the extrapolation of the thermal divergence of $\chi(T)$ and $\xi(T)$ leads to about the same value of T_c, as expected for critical phenomena. Figure 9 clearly shows that the virtual transition temperature, T_c, at which the critical fluctuations would diverge in absence of freezing, decreases with the Cs content, as expected from the decrease with x of the Coulomb repulsions between the Cs^+ ions.

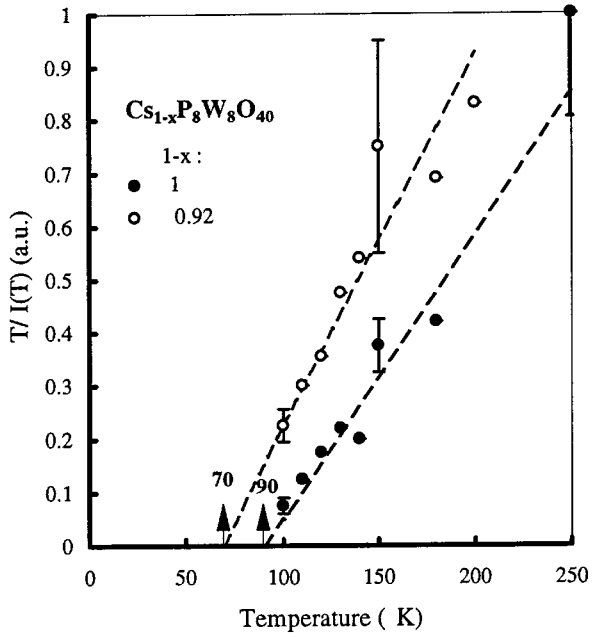

Fig. 9. Inverse of the $\mathbf{q}_s$ peak intensity corrected by the thermal population factor, $T/I(T)$, as a function of the temperature in $CsP_8W_8O_{40}$ and $Cs_{0.92}P_8W_8O_{40}$. The linear extrapolation allows us to define, according to equation (20), the virtual transition temperatures T_c of 90 K and 70 K, respectively.

5.2 Relationship with the charge transport properties

The electrical resistivity, $\rho(T)$ of $Cs_{1-x}P_8W_8O_{40}$ shows several interesting features [5–7].

i) for x small, its thermal coefficient ($d\rho/dT$) changes of sign at T_ρ. This coefficient is negative above T_ρ, and positive (as in a metal) below T_ρ until about 24 K, below which ρ increases steeply. T_ρ decreases when x increases.
ii) For x large (> 0.2) the thermal coefficient is negative over all the temperature range, and it decreases with decreasing temperature and increasing x.

The monotonous evolution of the resistivity with x, and the cooling and heating rate dependence of the resistivity of $Cs_{0.7}P_8W_8O_{40}$ [7], show that the Cs^+ ordering influences the charge transport properties. The change of sign of $d\rho/dT$ for x small, and its relative weak value for x large, suggest that $Cs_{1-x}P_8W_8O_{40}$ is on the borderline of a localization-delocalization Anderson transition [8] where the disorder, due to the Cs^+ sublattice, affects the electron mobility.

Let us first consider a 1D electron gas in the presence of randomly distributed impurities. In this simple case the 1D electron gas responds to the ~ 0 and $\sim 2\,k_F$ Fourier components of the potential created by the impurities. The first (second) Fourier component of the potential leads to a forward (backward) scattering of the electrons on the chain. Only the backward scattering leads to a localization of the electronic wave function [15]. In $Cs_{1-x}P_8W_8O_{40}$ the incompletely ordered Cs sublattice submits the electron gas, located on the W_4O_{18} double zig-zag chains, at a similar potential. In a purely 1D scenario, the Fourier components of the Cs^+ potential to be considered are those centered on q and spread over several $\xi_{//}^{-1}$ in the chain direction. In $Cs_{1-x}P_8W_8O_{40}$ this potential is quite weak because $q = \frac{1-x}{2}c^*$ corresponds to twice the $2k_F$ critical wave vector of the 1D electron gas. This feature and the fact that the Cs^+ ions are closer to the PO_4 groups than to the W_4O_{18} bichains, where the conduction electrons are located, explain why no strong localization effects are observed in all the Cs^+ concentration range. The increase of the localization effects when the Cs^+ content diminishes could be due to an enhancement of the $2k_F$ component of the Cs potential since the difference between q and $2k_F$ ($= \frac{1-x}{4}c^*$) diminishes and $\xi_{//}^{-1}$ increases when x increases.

The exact relation between the Cs ordering and the resistivity behavior is certainly more subtle to understand. In the purely 1D scenario where only the intrachain components of the potential created by the Cs sublattice are considered, the metallic like behavior observed below T_ρ could be associated with the net decrease of $\xi_{//}^{-1}$ observed below T_s. However a more realistic interpretation should take into account the 3D nature of the interaction of the electrons with the Cs^+ sublattice: the conduction electron cloud spread on the W_4O_{18} double zig-zag chains, which have a lateral extension, and each bichain is surrounded along **a** and **b** by 4 channels, partially filled by the Cs^+ ions, which provide the disordered potential. In other words, the Fourier dependence of the Cs^+ potential with wave vector components perpendicular to the channel direction should be considered, especially if their distribution varies because of the thermal variation of the interchannel ordering. At RT when the Cs^+ are only weakly ordered in channel direction the distribution of perpendicular wave vectors is very broad. It becomes narrower upon cooling when the Cs^+ order takes place between neighboring channels. In particular at a temperature T^* such that:

$$\xi_\perp(T^*) = d_\perp, \tag{21}$$

the first neighbor channels begin to be coupled and the electrons will experience a reduced disordered potential due to the local order of their surrounding. In agreement with this interpretation, it is interesting to remark that T^* is about 160 K in $CsP_8W_8O_{40}$ and 80 K in $Cs_{0.92}P_8W_8O_{40}$ (see Fig. 6), values which are close to those observed as a broad maximum in the resistivity, T_ρ, at about 160 K and 100 K respectively in samples of the same composition. Below T^* further reduction of the distribution of the Fourier components of the Cs^+ potential, due to the improved Cs^+ interchannel ordering, is probably important enough to weakly delocalize the conduction electrons. The metallic like behavior measured below T_ρ could thus be associated with this delocalized character of the electronic wave function on the W_4O_{18} bichains. As T^* cannot be defined in $Cs_{0.54}P_8W_8O_{40}$, no metallic like regime is observed for this concentration. This localization-delocalization crossover, associated with the local ordering of the Cs^+ concentration waves, involves only the charge degrees of freedom. Consequently the spin susceptibility does not present any anomaly at T_ρ [5,6].

As no additional reflections are observed at low temperature in the X-ray pattern, the steep increase of resistivity occurring below 24 K in $Cs_{1-x}P_8W_8O_{40}$ cannot be attributed to a CDW ground state or a CDW instability. Such increase of the resistivity has also been observed in the $Li_{0.9}Mo_6O_{17}$ [1a] molybdenum bronze and in the monophosphate tungsten bronzes $(PO_2)_4(WO_3)_{2m}$ with $m \geq 7$. In particular, in the $m = 8$ member, in agreement with the magnetoresistance measurements, this increase has been related to weak localization effects due to the absence of long range order in the CDW ground state [16]. The observed low temperature increase of the resistivity in the $Cs_{1-x}P_8W_8O_{40}$ could be similarly due to weak localization effects coming from the Cs disorder. This hypothesis is sustained by the observation of weak magnetoresistance effects similar to those observed in the $m = 8$ monophosphate tungsten bronze [7]. In addition, for a given disorder, one should expect stronger localization effects in the $Cs_{1-x}P_8W_8O_{40}$, which are 1D metals, than in $(PO_2)_4(WO_3)_{2m}$ which are 2D metals. Further studies are in progress, especially in the $m = 8$ monophosphate tungsten bronze, to better understand these low temperature weak localization phenomena.

However, as the degree of localization of the electronic wave function depends on the amount of interchannel disorder and as the interchannel coupling is mediated

through the P-W-O host lattice, the structural and electronic degrees of freedom do not behave independently. Their coupling is certainly highly non-linear, as suggested by the auto-catalytic like increase of $\xi_{//}$ observed below T_s in $CsP_8W_8O_{40}$ and in $Cs_{0.92}P_8W_8O_{40}$ when the interchannel interactions begin to set in. As noted above, the anisotropy of the correlation lengths seems to change dramatically with temperature and to play an important role in the electron localization process. Being 3D and quasi-isotropic below $\sim T_s$, the correlation length becomes 1D near RT. This surprising feature means that there is a thermal evolution of the interchain coupling. Near RT, it could be, because of the localized character of the electronic wave function on the W_4O_{18} bichains, that the dominant interchannel Coulomb interaction becomes direct in all the **a**, **b**, and $(\mathbf{a}+\mathbf{b})/2$ directions. As the direct interaction between two Cs^+ concentration waves tends to impose a phase shift of π, and as the channel network is triangular-like (see Fig. 8), a frustration in the phasing of the concentration waves could thus take place, improving the interchannel disorder. When upon cooling the chains are more polarizable, because the electronic wave function becomes more delocalized, the sign of the Coulomb interactions could change in the **a** and **b** directions where two channels sandwich a metallic bichain. With a zero phase shift in these directions the frustration effect is suppressed, setting the interchannel order described in part Section 4.2. Further work is necessary in order to analyze more quantitatively the feedback between the electronic and structural properties of $Cs_{1-x}P_8W_8O_{40}$.

6 Conclusion

We have performed a structural investigation of the $Cs_{1-x}P_8W_8O_{40}$ family of 1D inorganic conductors. We have shown that for x small a 3D ordering of the Cs sublattice occurs inside and between the octagonal channels delimited by the P-W-O host lattice. This order occurs on a limited spatial range whose magnitude decreases with decreasing Cs content. This ordering process has a dramatic effect on the charge transport properties of these materials. We believe that this is due to the 1D character of the electron gas of these tungsten bronzes. To our knowledge this is the first time in quasi-1D compounds that charge localization-delocalization phenomena of the Anderson type have been be so directly related with order-disorder structural effects. Somewhat similar features were previously reported in $Ag_{0.6}NbS_2$ [17]. This compound is a 2D metal which exhibits a structural transition where the Ag sublattice becomes ordered. In the ordered structure a net increase of conductivity is observed. However, probably because of the 2D character of its electron gas, and in contrast to the 1D case exhibited by $Cs_{1-x}P_8W_8O_{40}$, the high temperature disorder does not seem to change the delocalized nature of the electronic wave function in $Ag_{0.6}NbS_2$.

This work has benefited by useful discussions with S. Ravy, A. Rotgers and C. Schlenker.

References

1. For recent reviews see a) *Low Dimensional Electronic Properties of Molybdenum Bronzes and Oxides*, edited by C. Schlenker (Kluwer Academic Publisher, 1989). b) *Oxide Bronzes*, edited by M. Greenblatt, Int. J. Mod. Phys. **B23-24** (1993). c) *Physics and Chemistry of Low Dimensional Inorganic Conductors*, edited by C. Schlenker, J. Dumas, M. Greenblatt, S. Van Smaalen, NATO ASI B354 (Plenum Press, New York, 1996)
2. a) M. Greenblatt in reference [1b] p. 3937. b) B. Raveau, Proc. Indian Natn. Sci. Acad. **52**, 67 (1986); B. Raveau, Proc. Indian Natn. Sci. (Chem. Sci.) **96**, 4191 (1986).
3. Z.S. Teweldemedmin, R.V. Ramanujachary, M. Greenblatt, J. Solid State Chem. **95**, 21 (1991).
4. M. Goreaud, P. Labbe, B. Raveau, J. Solid State Chem. **56**, 41 (1985)
5. E. Wang, M. Greenblatt, J. Solid State Chem. **76**, 340 (1988).
6. E. Wang, M. Greenblatt, I. Rachidi, E. Canadell, M.H. Whangbo, Inorg. Chem. **28**, 2451 (1989).
7. A. Rotger, Thesis (University of Grenoble, 1993) unpublished.
8. See for example P.A. Lee, T.V. Ramakrishman, Rev. Mod. Phys. **57**, 287 (1985).
9. P. Foury, J.P. Pouget, E. Wang, M. Greenblatt, Synth. Met. **41-43**, 3973 (1991).
10. M.H. Whangbo, E. Canadell, Acc. Chem. Res. **22**, 375 (1989).
11. S.K. Khanna, J.P. Pouget, R. Comes, A.F. Garito, A.J. Heeger, Phys. Rev. B **16**, 1468 (1977).
12. A. Guinier, *X-Ray Diffraction in Crystals, Imperfect Crystals, and Amorphous Bodies* (Dover, 1994)
13. V.J. Emery, J.D. Axe, Phys. Rev. Lett. **40**, 1507 (1978).
14. P.A. Albouy, J.P. Pouget, H. Strzelecka, Phys. Rev. B **35**, 173 (1987).
15. See for example D. Jerome, H.J. Schulz, Adv. Phys. **31**, 299 (1982).
16. C. Hess, C. Le Touze, C. Schlenker, J. Dumas, D. Groult, J. Marcus, Synth. Met. **86**, 2419-2422 (1997).
17. A. Van Der Lee, S. Van Smaalen, G.A. Wiegers, J.L. De Boer, Phys. Rev. B **43**, 9420 (1991).